

Final Draft
of the original manuscript:

Zhang, N.; Said, A.; Wischke, C.; Kral, V.; Brodewolf, R.; Volz, P.;
Boreham, A.; Gerecke, C.; Li, W.; Neffe, A.T.; Kleuser, B.; Alexiev, U.;
Lendlein, A.; Schaefer-Korting, M.:

**Poly[acrylonitrile-co-(N-vinyl pyrrolidone)] nanoparticles –
Composition-dependent skin penetration enhancement of a dye
probe and biocompatibility**

In: European Journal of Pharmaceutics and Biopharmaceutics (2016) Elsevier

DOI: 10.1016/j.ejpb.2016.10.019

Poly[acrylonitrile-*co*-(*N*-vinyl pyrrolidone)] nanoparticles - Composition-dependent skin penetration enhancement of a dye probe and biocompatibility

Nan Zhang ¹, André Said ¹, Christian Wischke ^{2,3}, Vivian Kral ¹, Robert Brodwolf ^{3,4}, Pierre Volz ⁴, Alexander Boreham ⁴, Christian Gerecke ⁵, Wenzhong Li ², Axel T. Neffe ^{2,3}, Burkhard Kleuser ⁵, Ulrike Alexiev ^{4,5}, Andreas Lendlein ^{2,3}, Monika Schäfer-Korting ^{1,3,*}

1 Institute of Pharmacy, Freie Universität Berlin, Berlin, Germany

2 Institute of Biomaterial Science and Berlin-Brandenburg Center for Regenerative Therapies, Helmholtz-Zentrum Geesthacht, Teltow, Germany

3 Helmholtz Virtual Institute Multifunctional Biomaterials for Medicine, Helmholtz-Zentrum Geesthacht, Teltow, Germany

4 Institute of Physics, Freie Universität Berlin, Berlin, Germany

5 Institute of Nutritional Science, University of Potsdam, Germany

Corresponding author: Monika Schäfer-Korting, Institute of Pharmacy (Pharmacology and Toxicology), Freie Universität Berlin, Königin-Luise-Str. 2+4, D-14195 Berlin, Germany.
E-mail address: Monika.Schaefer-Korting@fu-berlin.de (M. Schäfer-Korting).

Keywords: Biocompatibility testing, Drug delivery systems, Nanoparticle, Poly[acrylonitrile-*co*-(*N*-vinyl pyrrolidone)], Polymers, Skin absorption

Abstract

Nanoparticles can improve topical drug delivery: size, surface properties and flexibility of polymer nanoparticles are defining its interaction with the skin. Only few studies have explored skin penetration for one series of structurally related polymer particles with systematic alteration of material composition. Here, a series of rigid poly[acrylonitrile-*co*-(*N*-vinyl pyrrolidone)] model nanoparticles stably loaded with Nile Red or Rhodamin B, respectively, was comprehensively studied for biocompatibility and functionality. Surface properties were altered by varying the molar content of hydrophilic NVP from 0 to 24.1% and particle size ranged from 35 to 244 nm. Whereas irritancy and genotoxicity were not revealed, lipophilic and hydrophilic nanoparticles taken up by keratinocytes affected cell viability. Skin absorption of the particles into viable skin *ex vivo* was studied using Nile Red as fluorescent probe. Whilst an intact stratum corneum efficiently prevented penetration, almost complete removal of the horny layer allowed nanoparticles of smaller size and hydrophilic particles to penetrate into viable epidermis and dermis.

Hence, systematic variations of nanoparticle properties allows gaining insights into critical criteria for biocompatibility and functionality of novel nanocarriers for topical drug delivery and risks associated with environmental exposure.

Introduction

The concept of topical drug delivery in skin diseases to enable almost exclusive desired local drug effects without side effects represents a well-established approach, which is expanded in current pharmaceutical research by studying various concepts ranging from hydrogels to vesicles, lipid particles, or nanocarriers from synthetic or biopolymers, which in some cases are combined with microneedles or other active principles to enhance drug penetration [1-6]. In all cases, the principle idea is to reduce the risk of systemic adverse effects and to overcome specific physicochemical barriers that limit the capacity of drugs to penetrate into the skin. Out of these concepts, nanoparticles with tailored particle size and surface properties are particularly promising candidates [7].

However, to date, only a few skin-targeting nanosystems have been introduced into the pharmaceutical praxis. The translation into clinical use is often challenged by limited stability of the nanoparticles and/or the inconsistent or unknown extent of particle penetration. The latter highly depends on the integrity of the physiological skin barrier function and thus is strongly influenced by regional variation of human skin, the stratum corneum in particular, as well as a disease related damage of the stratum corneum [8-11]. Apart from skin conditions, it is hypothesized that nanoparticles might interact with the lipid matrix of the skin or skin annexes and may gain access to deeper layers [12,13]. Thus, the individual characteristics of nanoparticles, such as size, rigidity/flexibility, shape, charge, or other surface modifications might additionally affect skin penetration of the nanoparticle, and if so, possibly induce toxic effects on keratinocytes and dermal fibroblasts [14,15]. This demands a critical evaluation of potential short- to long-term nanotoxicity. Therefore, detailed studies are required to identify the effect of nanoparticles on cellular function and penetration depth in human skin. While some studies compare carriers from different materials such as lipids and polymers [16], it would be of interest to explore nanoparticles from a single material system with systematic variation of properties [15,17].

Out of the various types of nanocarriers, polymer nanoparticles have long attracted the interest of researchers and are currently utilized in increasing numbers in medical and pharmaceutical applications. For dermal or transdermal delivery, particles from individual degradable or non-degradable polymers were studied [18-20], but altering polymer properties was neglected. Recently, a series of model nanoparticles composed of poly[acrylonitrile-*co*-(*N*-vinyl pyrrolidone)] [P(AN*co*NVP)] with increasing content of hydrophilic *N*-vinyl pyrrolidone (NVP), was explored for their surface properties, as well as cellular uptake by endothelial cells under inflammatory

conditions and particle bulk composition allowed to tailor biological effects [21,22].

Accordingly, the stably dye loaded P(ANcoNVP) nanoparticles were here selected and subjected to a comprehensive analysis of biocompatibility and penetration into human skin. The systematic characterization of uptake and transfer across physiological barriers, their irritancy potential, as well as induction of genotoxicity and/or cytotoxicity to exposed cells, should allow concluding on the effects of size and bulk nanoparticle composition on skin targeting capacity.

Materials and Methods

Nanoparticle synthesis and sample codes

The synthesis and characterization of nanoparticles involved the following chemicals: acrylonitrile (AN), *N*-vinyl pyrrolidone (NVP; both from Sigma-Aldrich, Taufkirchen, Germany, $\geq 99\%$ and purified prior to use), DMSO (Merck, Darmstadt, Germany), hexadecane ($\geq 99\%$, Fluka, Neu-Ulm, Germany), 2,2-azobis(2-methylbutyronitrile) (AMBN; 98%), sodium dodecyl sulfate (SDS; $\geq 98.5\%$), sodium tetradecyl sulfate (STS; $\geq 95\%$), sodium octadecyl sulfate (SOS; $\geq 95\%$), DMSO-*d*₆ and Nile Red (all from Sigma-Aldrich).

Poly[acrylonitrile-*co*-(*N*-vinyl pyrrolidone)] nanoparticles were synthesized by miniemulsion copolymerization as described in detail elsewhere [21,22]. Briefly, sonication was applied (Sonopuls HD 2017, Bandelin, Berlin, Germany) to prepare miniemulsions of monomer or comonomer mixture, hexadecane, AMBN, and Nile Red by dispersion in an aqueous phase containing either SDS, STS or SOS. The polymerization was initiated by heating to 77 °C under continuous steering in high pressure tubes. Diluted suspensions were purified by extensive dialysis (Visking type 20/32 membrane tubing, Carl Roth, Karlsruhe, Germany).

Polyacrylonitrile and poly[acrylonitrile-*co*-(*N*-vinyl pyrrolidone)] nanoparticles are here abbreviated as PAN and P(ANcoNVP) X, respectively, with X corresponding to the molar content of NVP units as determined by ¹H NMR spectroscopy. Additionally, samples with high loading of Nile Red dye are marked as NR^{high}, for samples with reduced particle size the size is indicated as ØZ [nm] with Z being the mean of the number averaged size distribution as determined by Scanning electron microscopy (SEM).

Characterization of nanoparticle properties

¹H NMR (500 MHz, Bruker, Bruker Biospin, Rheinstetten, Germany; method precision ± 3 mol%) was employed to analyze the composition of nanoparticles as described earlier [21]. The size of the particles and polydispersity index (PI) was determined by dynamic light scattering (DLS) using a

Zetasizer ZS (Malvern Instruments, Herrenberg, Germany; $n = 3$ measurements). SEM (Gemini SupraTM 40 VP, Carl Zeiss NTS, Oberkochen, Germany) was used to study particle size and structure with size determination by image analysis using AutoCAD ($n > 50$ particles, number-averaged size distribution).

The loading of Nile Red dye was determined by dissolution of lyophilized nanoparticles in 1 ml DMSO at 60 °C and fluorimetric quantification (Ex: 550 nm, Em: 600 nm; Infinity 200Pro, Tecan, Männedorf, Switzerland; $n \geq 6$ samples). Dialysis revealed no release of the payload out of the nanoparticles, confirming a stable entrapment of Nile Red.

Biological material

The use of human material/cells was approved by the ethics committee in charge. Normal human keratinocytes (NHK) and normal human dermal fibroblasts (NHDF) were isolated from juvenile foreskin after the parents signed the informed consent. NHK were expanded in low calcium keratinocyte growth medium (KGM BulletKit, Lonza, Cologne, Germany). NHDF were cultivated in Dulbecco's Modified Eagle Medium (DMEM, Sigma-Aldrich), supplemented with 7.5% fetal calf serum (FCS), L-glutamine (5 mM), 100 I.U./ml penicillin and 100 µg/ml streptomycin (Biochrom, Berlin, Germany). Human skin for penetration studies was obtained from patients who underwent abdominal reduction surgery after informed consent was signed. Human skin was treated and stored as described previously [8]. Red blood cells (RBCs) were obtained from buffy-coat donations from anonymous healthy volunteers (DRK-Blutspendedienst Ost, Berlin, Germany). Bovine eyes for assessment of irritation potential were obtained from freshly slaughtered cattle (Teterower Fleisch, Teterow, Germany) after approval of the veterinary inspection office.

Cytotoxicity studies

The cytotoxic effects of nanoparticles were determined by 3-(4,5-dimethylthiazol-2-yl)-2,5-diphenyltetrazolium bromide (MTT) reduction assay [15] as well as Trypan blue exclusion test [23]. Briefly, NHK and NHDF at a density of 10^4 cells per well were incubated with nanoparticles at concentration of 0.05% and 0.005% [w/v] in KGM or complete DMEM without FCS, respectively, for 24 h or 48 h. MTT solution was added and the absorbance was measured at 540 nm (FLUOstar Optima, BMG Labtech, Offenburg, Germany). Respective media were used as reference for untreated cells, 0.005% [w/v] SDS served as positive control and 0.005% [v/v] distilled water as solvent control. Cell viability below 75% predicts cytotoxic effects.

For assessment of membrane integrity, NHK and NHDF at the density of 10^4 cells were incubated with nanoparticles 0.05% [w/v] in KGM or complete DMEM without FCS, respectively, for 24 h. 10 μ L of Trypan blue (0.04%, Sigma-Aldrich) were added and after 1 min cells were washed twice with PBS. 5 images per sample were captured under an inverted light microscope (Axiovert 135, Carl Zeiss, Jena, Germany). Three independent experiments were performed and a minimum of 100 cells per sample were classified as viable or nonviable.

Alkaline single-cell gel electrophoresis (Comet assay) and Determination of ROS induction

For the alkaline single-cell gel electrophoresis (Comet assay) procedure [15], 3×10^5 NHK or NHDF were incubated with nanoparticles 0.05% [w/v] for 24 h, harvested and re-suspended with 1% low-melting point agarose. 50 cells per slide and 3 slides per treatment were examined by Lucia Comet Assay SoftwareTM (Lucia Cytogenetics, Prague, Czechia). DNA damage was expressed as the relative tail length.

Intracellular reactive oxygen species (ROS) levels were determined by 6-Carboxy-2',7'-dichlorodihydrofluorescein diacetate (H2DCFDA) assay [24]. NHK and NHDF at a density of 5×10^4 cells were incubated for 1 h with nanoparticles 0.05% [w/v] in KGM or DMEM without FCS, respectively, and after washing incubated with 25 μ M H2DCFDA for 1 h and analyzed on a FACSCanto II (BD Biosciences, Heidelberg, Germany). FlowJo software (Treestar, Ashland, OR, USA) was used for data analysis. Dead cells and debris were excluded by forward/sideward scatter plot.

For the comet assay and ROS determination, PBS (10%) in KGM or DMEM without FCS, respectively, served as negative control, silver (Ag) nanoparticles (diameter 40 nm, 5 μ g/ml, Sigma-Aldrich) served as positive control.

Fluorescence life time imaging microscopy (FLIM) for cellular uptake studies

For fluorescence lifetime imaging microscopy (FLIM) measurements, NHK were incubated for 1 h and 24 h at 37 °C and 5% CO₂ with Nile Red loaded P(ANcoNVP) nanoparticles at a concentration of 0.005 and 0.006% [w/v], respectively. NHK were seeded into glass bottom chambers (CELLviewTM, Greiner Bio One, Kremsmuenster, Austria) at a concentration of 3×10^5 cells per 300 μ l KGM or 1.5×10^5 NHK in 750 μ l KGM, respectively. In order to stain cell nuclei, NHK were incubated with 4',6-Diamidin-2-phenylindol (DAPI, Dianova, Hamburg, Germany) within the glass bottom chambers at a concentration of 28.3 μ M. In addition, CellMaskTM deep red (CMDR,

Molecular Probes, Eugene, OR USA) was used to stain cell membranes by adding CMDR to a final concentration of 1 µg/ml. FLIM experiments were performed in the time-domain using time correlated single photon counting (TCSPC) [25].

The used FLIM setup consists of an inverted microscope (IX71, Olympus, Hamburg, Germany) equipped with a 60× objective lens (UPLSAPO60XW, Olympus), a galvo scanner unit (DCS-120, Becker & Hickl, Berlin, Germany) for laser scanning and a picosecond tunable white light supercontinuum laser source in combination with an acousto-optical tunable filter (SuperK Extreme EUV3 and SELECT UV-vis, NKT Photonics A/S, Blokken, Denmark) for Nile Red and CMDR or a pulsed diode laser (DAPI) (BDL-405-SMT; Becker & Hickl) for DAPI excitation, respectively [26-28]. Nile Red fluorescence was excited at 530 nm at a pulse repetition rate of 19.5 MHz. The resulting fluorescence emission was spectrally selected by a long-pass filter (HQ 545 LP, Chroma, Bellows Falls, VT, USA) [29]. CMDR fluorescence excitation was at 640 nm with a repetition rate of 19.5 MHz and corresponding CMDR fluorescence emission was detected above 665 nm using a long-pass filter (665 LP ET, Chroma). To excite DAPI fluorescence, a diode laser at 405 nm with a pulse repetition rate of 20 MHz was used. DAPI fluorescence is collected between 430 and 475 nm by using a bandpass filter (452/45 BrightLine HC, Semrock, Rochester, NY, USA). The ratio of the stop/start pulse rate was normally less than 200:1, appropriate for single photon counting [30,31]. A FLIM image consist of 512 × 512 px, in each pixel fluorescence decay traces were collected in 1024 time channels with a channel width of 19.5 ps by using a hybrid PMT (HPM-100-40) and a TCSPC module (SPC-160, both from Becker & Hickl). The instrument response function of the system was less than 100 ps full width at half maximum.

Irritation potential

The bovine corneal opacity and permeability (BCOP) test was performed according to OECD guideline 437 [32]. Briefly, the cornea of bovine eyes was isolated and washed in Hanks' Balanced Salt Solution (HBSS with Ca²⁺ and Mg²⁺) mounted in the cornea holders with Minimum Essential Medium (MEM, without Phenol Red; both from Gibco by Life Technologies™, Carlsbad, CA, USA) and measured for initial opacity after 1 h (Opacitometer Kit, BASF-OP 3.0, Ludwigshafen, Germany). Nanoparticles at a concentration of 0.05% [w/v] were added for a period of 10 min, and final opacity was measured after 4 h. Permeability was determined by adding sodium Fluorescein solution (4 mg/mL, Sigma-Aldrich). Spectrophotometric measurements (WPA Biowave, Biochrom, Cambridge, UK) evaluated at 490 nm were recorded as optical density (OD490). De-

ionized water was used as negative control, 100% [v/v] ethanol (VWR, Darmstadt, Germany) as positive control and Titanium Dioxide (TiO₂) (<150 nm, Sigma-Aldrich) 0.05% [w/v] in de-ionized water as particulate control. The final *in vitro* irritancy score (IVIS) was calculated with the equation: IVIS = mean opacity value + (15 × mean permeability OD490 value).

Red blood cell (RBC) test was performed according to INVITTOX N°37 protocol [33]. RBC diluted with 10 mM glucose (Sigma-Aldrich) to 4 × 10⁹ cells/mL was added to nanoparticles in PBS. De-ionized water served as positive control, PBS as negative control and SDS solutions ranging in concentrations from 0 to 80 ppm as hemolysis reference. The absorbance of the released oxyhemoglobin at 560 nm (WPA Biowave, Biochrom) was measured and the relation between effective concentration of 50% hemolysis and protein denaturation was calculated to evaluate acute eye irritancy potential.

Skin penetration studies

The penetration of Nile Red loaded P(ANcoNVP) nanoparticles was evaluated using the Franz cell setup [34] and cryoconserved human skin. The particles were studied in parallel on skin from the same (in total 3) donors. For damaged skin, 90% of the stratum corneum was removed by tape stripping for 40 times, assessed by histology and thickness measurement. The procedures are specified elsewhere in detail [15]. Briefly, 35 µL of the nanoparticles formulation was applied for 6 h, the treated skin areas were then embedded in tissue freezing medium (Jung, Nussloch, Germany) and stored at 80 °C. Analysis of skin slices and determination of fluorescence detection limit (BZ-8000, BZ Analyser software, Keyence, Neu-Isenburg, Germany) was performed as described previously [35]. The pixel brightness values (arbitrary brightness units, ABU) were recorded in the viable epidermis and dermis to semi-quantitatively determine the amount of Nile Red. In total, 2 sections from one skin for each of the 3 different donors (in total 6) were analyzed and the average intensity value was normalized according to the dye loading of respective nanoparticles.

Statistical analysis

Data are depicted as mean ± SEM. Statistical significance of differences was determined by one-sample *t*-test or one-way analysis of variance (ANOVA) followed by a Bonferroni post hoc analysis and considered significant at $p \leq 0.05$. Statistical analysis was performed using GraphPad Prism 5.0 (GraphPad software, La Jolla, CA, USA).

Results and discussion

Here we studied the functionality and biocompatibility of a series of P(ANcoNVP) nanoparticles with defined modifications of the matrix composition.

Composition and properties of P(ANcoNVP) nanoparticles

The capacity of miniemulsion copolymerization to produce homogeneously sized nanoparticles is based on high stability of the oil-in-water emulsion droplets when using a charged surfactant, typically SDS, and a hydrophobic costabilizer such as hexadecane to reduce the Laplace pressure and retard the Ostwald ripening [36]. As illustrated in Table 1, particles with low polydispersity indices (PDI) were obtained as detected by DLS analysis. When using SDS as surfactant, the mean particle size adapted values in the range of 170-220 nm for the different batches as it is characteristic for this process [21,22]. The content of hydrophilic NVP varied between 0 mol% and 24 mol% as confirmed by ¹H NMR spectroscopy. Extensive dialysis, as previously shown, allowed removing SDS excess with final contents in the low ppm range to exclude surfactant induced cell effects [21]. In order to prepare smaller sized emulsion droplets and thus smaller nanoparticles, the hydrophobicity of the surfactant was increased by replacing SDS by tensides with longer and more hydrophobic alkyl chains, namely STS and SOS. In this way, a series of particles with similar NVP content but decreasing size was obtained, namely P(ANcoNVP)14, P(ANcoNVP)16 Ø51, and P(ANcoNVP)17 Ø36 (Fig. 1). While DLS analysis indicated some aggregation based on particle sizes and PDI, electron microscopy confirmed very small primary particle sizes in the range of 51 ± 11 nm and ~36 ± 5 nm, respectively.

In order to allow studying the particle behavior in biological environments such as their penetration in human skin, all nanoparticles were labelled by incorporating Nile Red during miniemulsion copolymerization at concentrations of 59-73 ng per mg nanoparticles as quantified by particle drying, dissolution, and fluorimetric detection of the dye. For high sensitivity detection, an additional set of nanoparticles were included with elevated dye payload [PAN-NR^{high}, P(ANcoNVP)24-NR^{high}]. For some experiments, including cytotoxicity assessment by MTT, P(ANcoNVP) loaded with Rhodamine B (RhoB) were used as reference particles [22].

Table 1

Composition and properties of P(ANcoNVP) nanoparticles.

Sample code ^a	Synthesis Surfactant type ^b	Composition NVP content (mol%) ^c	Particle size		Payload Nile Red (ng/mg)
			DLS Z-Average/PDI (nm)/-	SEM ^d (nm)	
PAN	SDS	0	219/0.057	208 ± 28	57
P(ANcoNVP)0.1	SDS	0.1	194/0.014	161 ± 15	71
P(ANcoNVP)14	SDS	14.0	174/0.026	139 ± 16	66
P(ANcoNVP)16 Ø51 nm	STS	15.8	(132/0.222) ^e	51 ± 11	59
P(ANcoNVP)17 Ø36 nm	SOS	16.6	(98/0.229) ^e	36 ± 5	73
PAN-NR ^{high}	SDS	0	237/0.046	216 ± 33	749
P(ANcoNVP)24-NR ^{high}	SDS	24.1	176/0.091	133 ± 13	2335

^a Sample code: PAN = Nanoparticles synthesized only with acrylonitrile as repetitive unit; P(ANcoNVP) X = copolymer nanoparticles with X corresponding to the determined molar NVP content. Samples with high loading of Nile Red dye are marked as NR^{high}. Samples with reduced particle size are indicated as ØZ with Z being the mean of the number averaged size distribution as determined by SEM [nm].

^b SDS = sodium dodecyl sulfate, STS = sodium tetradecyl sulfate, SOS = sodium octadecyl sulfate.

^c Determined by NMR with typical precision of ±3 mol-%.

^d SEM size data correspond to the mean and standard deviation of the number distribution.

^e Artefacts due to aggregates remaining after 15 s treatment in an ultrasound bath.

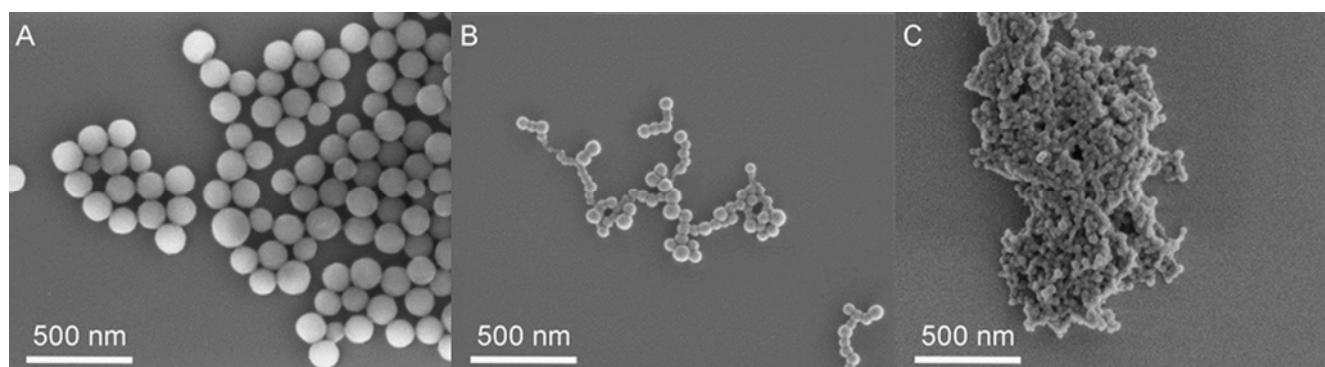


Figure 1. Exemplary electron microscopy images illustrating the tailoring of particle sizes of (A) PANcoNVP 14, (B) PANcoNVP 16 Ø51 and (C) PANcoNVP 17 Ø36. Scale bar represents 500 nm as depicted.

Cytotoxicity

Nanotoxicity can be roughly classified into acute and chronic effects. Acute toxicity includes immediate cell death, reduction in metabolic activity and inflammation, whereas chronic toxicity generally refers to genotoxicity and carcinogenesis [37], besides enhanced efficacy because of

accumulation of the substance. To assess the potential interaction of the nanoparticles of interest with cutaneous cells in relation to concentration and exposure time, we first performed MTT assay on primary NHK and NHDF (Fig. 2A and B). For nanoparticles of intermediate NVP content, P(ANcoNVP)14 and P(ANcoNVP)16 Ø51, good biocompatibility was confirmed for NHK. In case of P(ANcoNVP)17 Ø36 with comparable hydrophilicity but smaller size, an increased cytotoxicity was observed in NHK at higher concentrations. Additionally, the hydrophobic PAN, P(ANcoNVP)0.1 and PAN-NR^{high} nanoparticles appeared more cytotoxic in NHK after 24 h and 48 h, particularly when used at higher concentration of 0.05%, than the similar sized P(ANcoNVP)14 nanoparticles with intermediate NVP content, indicating that hydrophilicity can have a direct impact on cell viability. For NHDF, overall no decrease in viability was observed.

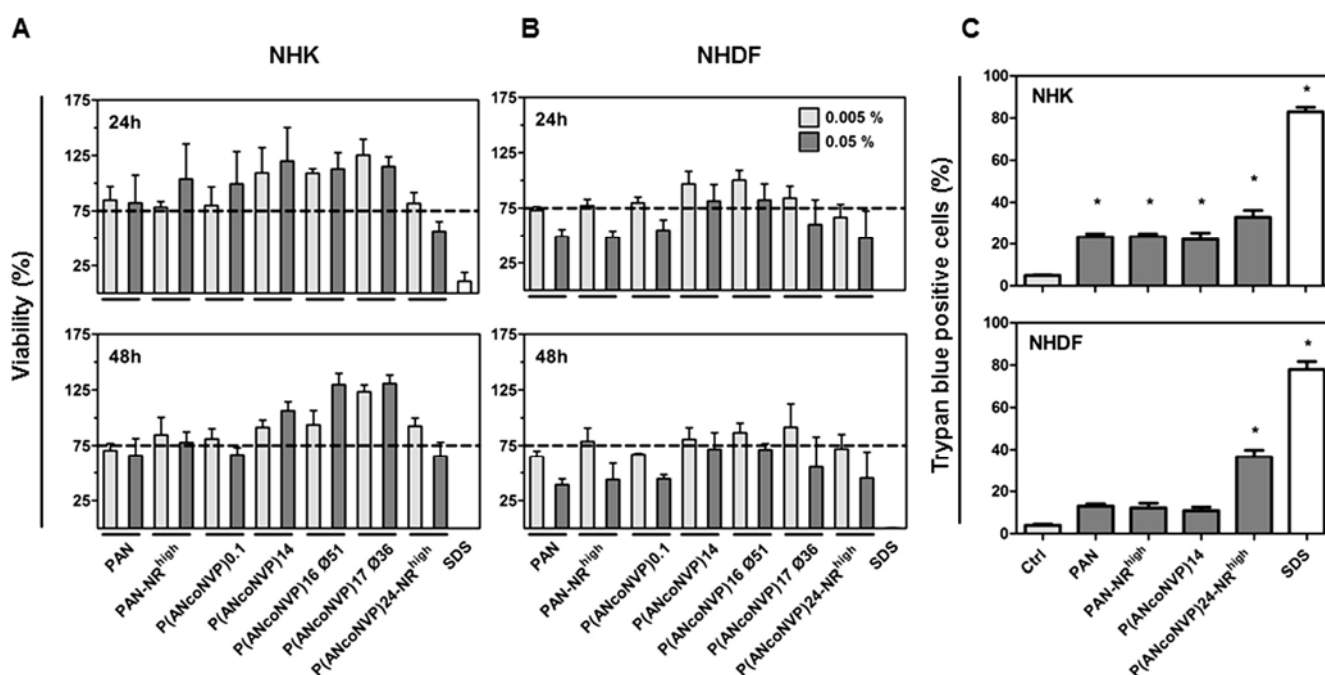


Figure 2. Assessment of cytotoxicity. Viability of (A) normal human keratinocytes (NHK) and (B) dermal fibroblasts (NHDF) following exposure to P(ANcoNVP) nanoparticles or SDS for 24 and 48 h, respectively, was determined by MTT assay. Mean \pm SEM (n = 3). Trypan blue incorporation of (C) NHK and NHDF following exposure to selected P(ANcoNVP) nanoparticles or SDS for 24 h, respectively. Mean \pm SEM (n = 3). * $p \leq 0.05$, ANOVA with post hoc Bonferroni test.

For P(ANcoNVP)24-NR^{high}, which exhibits a 35-fold higher dye loading, the slightly reduced viability of NHK might be referred to the dye payload rather than the polymer composition. It should be noted that no cytotoxicity was observed in a control experiment with P(ANcoNVP) nanoparticles varying in 0, 16.5 and 21.5 mol% NVP, loaded with the hydrophilic dye Rho B (Suppl. Table S1, Fig. S1). However, by assessing the cytotoxic effect of soluble Nile Red solution (diluted in methanol) in concentrations up to 0.0003% [w/v], representing the calculated dye amount

in P(ANcoNVP)24-NR^{high} nanoparticles, no decrease of viability (>93% for 48 h) was obtained for NHK and NHDF, respectively.

Yet, as each cell viability or cytotoxicity assay only refers to a single endpoint, a combination of validated *in vitro* tests appears mandatory to understand the potential hazard mediated by nanoparticles. Indeed, the tetrazolium based MTT assay appears to be affected by a range of different nanoparticles, resulting in either substantial over- or under-estimations of toxicity [38-40]. Possible interactions of nanoparticles with the accuracy of toxicity tests include their intrinsic fluorescence/absorbance or their interference with assay components. Thus, the membrane integrity of exposed cells after 24 h was additionally assessed by trypan blue exclusion assay (Fig. 2C). With PAN, PAN-NR^{high}, P(ANcoNVP)14 and P(ANcoNVP)24-NR^{high} similar sized nanoparticles with increasing hydrophilicity were investigated and revealed an enhanced incorporation of trypan blue into NHK and NHDF, with P(ANcoNVP)24-NR^{high} showing the highest dye uptake. Thereby, the previously observed cytotoxicity of P(ANcoNVP) nanoparticles in concentrations of 0.05% were largely confirmed, and the validity of our data obtained by MTT assay was approved.

The above mentioned observations of size-dependent tolerability in part were expected, since smaller particles are generally considered to be more reactive due to increased specific surface area, potentially inducing larger toxicological effects, irrespective of the matrix composition [26,41]. However, regarding the hydrophilicity, the exposure of P(ANcoNVP) nanoparticles to human umbilical vein endothelial cells (HUVECs) revealed the highest tolerability for nanoparticles containing above 20 mol% NVP, whereas more lipophilic particles affected viability in a concentration-dependent manner [19]. These rather contrasting outcomes might be explained by the different cell types. In fact, NHK generally appear much more sensitive to nanoparticles compared to NHDF, resulting in decreased values for cell viability after 24 h and 48 h, respectively [15,17]. This holds also true for the respective immortalized cell lines [15,42] and might be due to differences in metabolic activity, defining the cell-specific susceptibility to endogenous or exogenous stimuli. Additionally, the relative increase of viability (above 125%) in exposed NHDF in the MTT test, as observed for smaller sized P(ANcoNVP)17 Ø36 and P(ANcoNVP) 16 Ø51 nanoparticles should refer to elevated stress-induced mitochondrial activity, thus indicating the onset of toxicity and finally cell death.

To date, the mechanistic explanation for the different tolerability of P(ANcoNVP) nanoparticles, either loaded with Nile Red or RhoB, is missing and will be determined in future studies. An influence of intracellular deposition of the dye by particle uptake, of particle surface hydrophilicity

or potentially osmotic properties of nanoparticles, might be possible considering the nature and/or amount of the entrapped payload while SEM analysis of the particles does not indicate structural differences.

As exposure of P(ANcoNVP) nanoparticles can on the one hand be associated with altered cell viability, depending on the individual matrix composition and particle size, and on the other hand, can be accompanied with a general increase of cell permeability, this leads to the assumption, that P(ANcoNVP) nanoparticles, by interacting with cell membranes, might be internalized and possibly exert cytotoxic effects upon uptake.

Fluorescence life time imaging microscopy (FLIM)

In order to test the assumption that the above described cytotoxic effects are connected to cellular uptake of the P(ANcoNVP) nanoparticles, we performed raster-scanning based FLIM experiments to visualize the localization of nanoparticles after exposure to NHK. With PAN-NR^{high}, P(ANcoNVP)14 and P(ANcoNVP)24-NR^{high}, similar sized nanoparticles were chosen with increasing NVP content. Using a cluster-based FLIM image analysis, the localization of Nile Red as the nanoparticle reporter dye was identified within NHK after 24 h incubation (Fig. 3). Cellular uptake was more pronounced after 24 h compared to 1 h incubation (Suppl. Fig. S2), in particular for PAN-NR^{high} and P(ANcoNVP)14. Based on the differential distribution of Nile Red loaded nanoparticles (Fig. 3A-C) and free Nile Red (Fig. 3D) in NHK, we conclude that upon cellular uptake probably no release of the dye from the nanoparticles occurs. Thus, Nile Red mirrors the distribution of the respective nanoparticles.

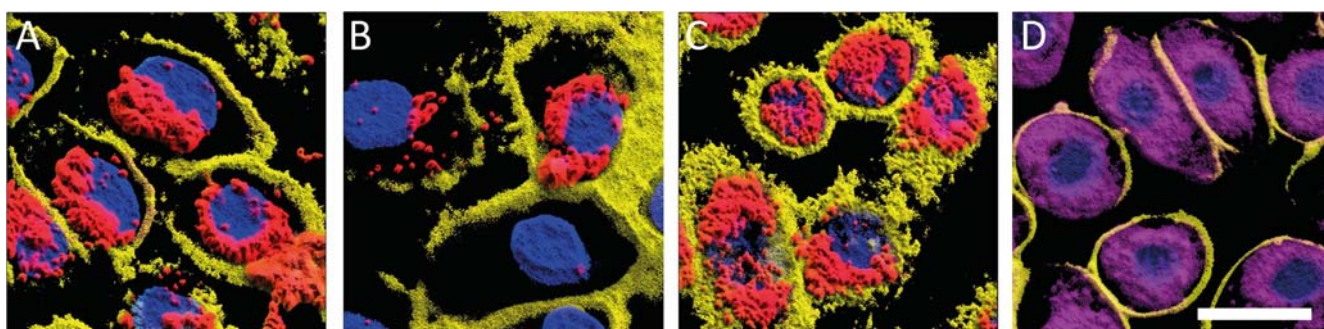


Figure 3. Cellular uptake of P(ANcoNVP) nanoparticles with increasing hydrophilicity as revealed by fluorescence life time imaging microscopy (FLIM). False color images of NHK after 24 h exposure to (A) PAN-NR^{high}, (B) P(ANcoNVP)14 and (C) P(ANcoNVP)24-NR^{high} nanoparticles. Red: nanoparticles (signal of encapsulated Nile Red); Blue: DAPI staining of cell nuclei; Yellow: CMDR staining of cell membranes. (D) False color images of NHK after 24 h exposure to free Nile Red (magenta). Scale bar represents 20 μm . (For interpretation of the references to colour in this figure legend, the reader is referred to the web version of this article.)

To date, the influence of hydrophilicity on the internalization of polymeric nanoparticles is poorly investigated. Recent findings revealed a major enhancement of cellular uptake of poly(L-lactide) nanoparticles by increasing the hydrophobicity through copolymerization with membrane lipid components, thus imitating the hydrophobic nature of cell membranes [43]. Indeed, the uptake of the hydrophobic nanoparticles by NHK after 24 h appears to be more pronounced compared to P(ANcoNVP)14. Nevertheless, the most hydrophilic nanoparticles P(ANcoNVP)24-NR^{high} showed the strongest uptake. Since the amount of incorporated dye was also the highest for these nanoparticles, the higher visibility within NHK might be due to the higher dye load. On the other hand, as discussed in the context of cell viability results, the different dye payloads might possibly affect the interaction of the nanoparticles with NHK. This is corroborated by the fact that both cellular uptake images and observed cell viability after 24 h (Figs. 2A and C, 3, Suppl. Fig. S1) showed a similar dependence. Control experiments with Rhodamin B loaded P(ANcoNVP) nanoparticles with low dye payload also revealed cellular uptake after 24 h (data not shown), albeit the amount of nanoparticles taken up differs less compared to the Nile Red loaded nanoparticles. It is currently unclear whether the described uptake of P(ANcoNVP) nanoparticles is either facilitated due to ongoing cell death, or the internalization of nanoparticles is a prerequisite for cytotoxicity. Nevertheless, the matrix composition of polymer nanoparticles seems to define the extent of cell interaction and thus has to be taken into account for possible mechanisms of skin penetration characteristics, but additionally, effects of the very high dye loading, especially for P(ANcoNVP)24-NR^{high} nanoparticles cannot be excluded, thus further investigations are needed in future.

Anyhow, since FLIM measurement confirmed that P(ANcoNVP) nanoparticles exhibit the capacity to enter NHK (Fig. 3), it was assessed whether the uptake of nanoparticles and the observed cytotoxic effects were accompanied by induction of ROS production and DNA damage.

Genotoxicity and induction of ROS

Oxidative stress, frequently observed with metal-based nanoparticles, orchestrates a series of pathological events such as genotoxicity and apoptosis. Intracellular ROS production occurs mainly as byproduct of the mitochondrial respiratory chain or through cell membrane NADPH oxidase, inducing damage of DNA and other macromolecules [44,45]. Ag nanoparticles used as positive control induced a significant ROS production in NHK and NHDF within 1 h after exposure (Fig. 4B). The mitochondrial ROS production and subsequent promotion of intrinsic apoptotic pathways

by Ag nanoparticles is assumed to be caused after cellular internalization, whilst the exact uptake mechanisms are yet unclear [46]. In contrast, P(ANcoNVP) nanoparticles neither induced ROS production nor significant DNA damage as shown by Comet assay in NHK and NHDF, except for the most hydrophilic P(ANcoNVP)24-NR^{high} revealing elevated ROS levels in NHDF within 1 h (Fig. 4A and B). In fact, although ROS generation is a common occurrence during induced toxicity and therefore has to be intensively characterized in order to predict biocompatibility of nanoparticles, ROS generation is not a definite prerequisite for cytotoxicity. Previous studies already reported direct cytotoxic effects of nanoparticles without stimulating ROS production [47,48].

The lack of considerable genotoxicity or induction of ROS by most P(ANcoNVP) nanoparticles suggests, that the cytotoxic effects for some compositions as reported above are likely based on a local disturbance of cell integrity, possibly caused by hydrophobic and/ or hydrophilic interactions with cell membranes, without necessarily stimulating a direct or indirect cellular stress response.

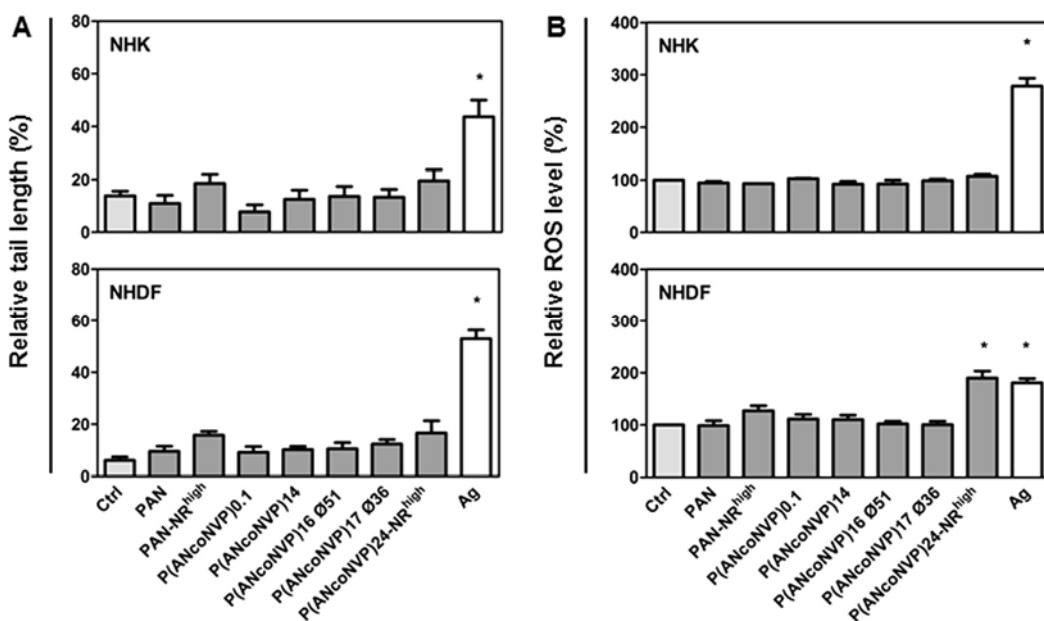


Figure 4. Analysis of genotoxicity and ROS induction. (A) Comet assay of NHK and NHDF following exposure to P(ANcoNVP) nanoparticles or Ag nanoparticles for 24 h. DNA damage is depicted as relative tail length (%) Mean \pm SEM (n = 3). * $p \leq 0.05$, ANOVA with post hoc Bonferroni test. (B) Induction of cellular reactive oxygen species (ROS) in NHK and NHDF after 1 h exposure to P(ANcoNVP) nanoparticles or Ag nanoparticles. Relative ROS levels were quantified by ROS assay. Mean \pm SEM (n = 3) * $p \leq 0.05$, one-sample *t*-test, with PBS (10%) in KGM or DMEM without FCS, respectively, as control.

Irritation potential

Besides cell compatibility studies with isolated cells, a comprehensive nanotoxicological investigation requires the analysis of tissue interaction, here particularly of tissues exposed at the body surface. Since (un)intentional ocular exposure of nanoparticles used for topical drug delivery or in cosmetic products may induce damage, the evaluation of eye irritation is essential [49,50]. In order to assess the irritation potential of P(ANcoNVP), the BCOP assay (OECD TG 437), classified as an organotypic *ex vivo* method, and the *in vitro* RBC test (INVITTOX No. 37) were conducted, both validated alternative test systems aiming to replace the original reference method, the *in vivo* Draize eye irritation test (OECD TG 405) [32,33,51]. SDS served as hemolysis reference for the RBC test, where the disruption of the cell membranes in freshly isolated red blood cells induces hemoglobin leakage. 50% hemolysis was observed with a concentration of 29 ppm SDS, whereas the tested P(ANcoNVP) in concentrations up to 0.05% (w/v), showed negligible hemolysis (Fig. 5A and B).

The BCOP assay was performed in accordance to the OECD guideline 437, calculating an *in vitro* irritation score (IVIS) to classify the test substance into “No Category” (≤ 3), “No prediction can be made” ($>3; \leq 55$) and “Category 1”, inducing serious eye damage (>55), as defined by the United Nations Globally Harmonized System of Classification and Labelling of Chemicals (UN GHS) [32]. Ethanol served as positive control (IVIS value of around 118). The TiO₂ nanoparticles as particulate reference, formerly reported to exert slight eye irritating effects and to be applicable for the BCOP assay [52,53], fell here into the category of “No prediction can be made” with the IVIS value of 26.8 (Fig. 5C). However, all tested P(ANcoNVP) nanoparticles revealed IVIS values of less than 3 and thus can be classified as “No Category”. These results clearly indicate that P(ANcoNVP) nanoparticles are devoid of irritating potential for the eye, irrespective of individual size and matrix composition. Yet, the use of *ex vivo* or *in vitro* methods face distinct limitations, since both the RBC test and BCOP assay are not able to assess the full spectrum of the GHS categories. At present, no alternative test system is able to fully replace the *in vivo* Draize eye irritation test in its capacity to differentiate between UN GHS Category 1 (serious eye damage) and UN GHS Category 2 (eye irritation) [54]. Nevertheless, by using TiO₂ as a nanoparticle reference with known eye irritation potential, the direct comparison of the polymer-based nanoparticles to these anorganic nanoparticles confirmed that P(ANcoNVP) lack undesired severe irritating effects.

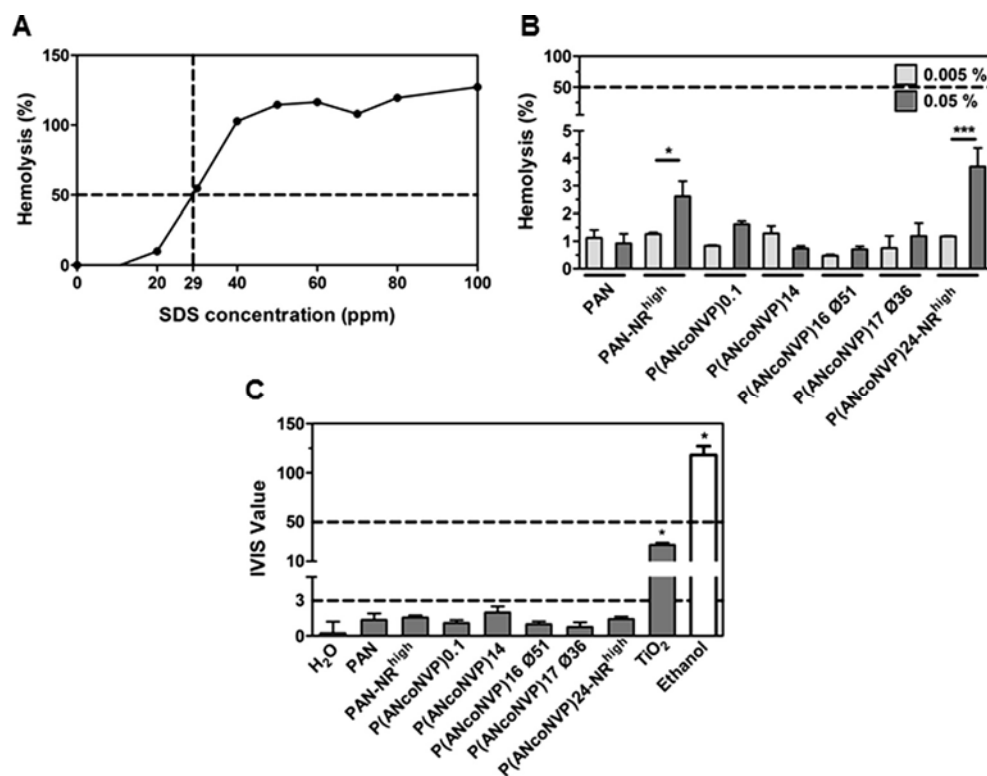


Figure 5. Assessment of eye irritation potential of P(ANcoNVP) nanoparticles. (A) Concentration-dependent increase of hemolysis (%) of red blood cells by SDS as reference determined by RBC assay. (B) Induced hemolysis (%) by P(ANcoNVP) nanoparticles after 10 min. Mean \pm SEM (n = 2-3). (C) Opacity increase and permeability decrease of bovine corneas after incubation with P(ANcoNVP) nanoparticles. TiO₂ nanoparticles served as particulate reference. The final *in vitro* irritancy score (IVIS) was calculated and is depicted as Mean \pm SEM. (n = 3) **p* < 0.05, ****p* < 0.001 ANOVA with post hoc Bonferroni test.

Skin penetration studies

The systematic variation of nanoparticle properties allowed gaining insights into critical criteria for the biocompatibility of polymeric nanoparticles, whereas their functionality as novel dermal or transdermal delivery system is determined by the penetration behavior. Human skin is known to be relatively penetrable for moderate lipophilic substances not $>600 \text{ g mol}^{-1}$ [34], whereas the P(ANcoNVP) model nanoparticles were of much larger size and varied in hydrophilicity. The penetration studies on P(ANcoNVP) nanoparticles with stably encapsulated Nile Red allowed us to characterize the transport of the nanoparticles into human skin *ex vivo* since Nile Red presumably remains trapped in the particles within the duration of the penetration experiment. Interestingly, irrespective of the individual size and matrix composition, all of the tested P(ANcoNVP) nanoparticles accumulated exclusively in the outermost layer of the stratum corneum, indicating no penetration into deeper skin layers after 6 h of exposure (data not shown). Considering the function

of the stratum corneum, together with the specific content, composition and structure of the stratum corneum lipids [55], as limiting barrier against percutaneous penetration, these data confirm that the analyzed nanoparticles may not be able to enter viable skin, which is well in accordance to the absent penetration of rigid nanoparticles (<200 nm) reported before [17,19,56,57].

However, the physical skin barrier is likely compromised in damaged or diseased skin, which may be susceptible for drug transport by nanoparticulate delivery systems as well as for the uptake of the nanoparticles. When removing 90% of the stratum corneum by tape stripping, mimicking a lesional state of human skin, such as contact dermatitis [58], clearly enhanced penetration was observed as suggested by fluorescence signals detected in the viable epidermis after 6 h (Fig. 6). In more detail, P(ANcoNVP)16 Ø51 and P(ANcoNVP)17 Ø36, representing nanoparticles of small size, and P(ANcoNVP)24-NR^{high}, the most hydrophilic nanoparticle with high dye payload for increased sensitivity of detection, were observed to enter also the dermis, which confirmed the assumed dependence of size and matrix composition for skin penetration behavior. Regarding the individual nanoparticle characteristics, different penetration routes are conceivable, in particular the intercellular route for nanoparticles of small size or - less likely - the transcellular route for those showing substantial cell uptake. In addition, the higher content of NVP reduces surface roughness of nanoparticles [21,22] and might increase their softness in the water-swollen state, facilitating penetration due to gained flexibility, as it has been confirmed previously for liposomes [59].

Although conceived as a semi-quantitative approach, a critical limitation of such penetration study is always the respective payload of dye that enables quantification. The detection limit of fluorescence signals was assessed and quantified to be 0.003 ng ml⁻¹ Nile Red [35]. Considering the different payloads (Table 1), the measured arbitrary pixel brightness units (ABU) were normalized to the determined individual payload of Nile Red. Still, this process might include a systemic bias due to propagation of uncertainties and sensitivity of the respective detection method. Furthermore, as the set of NR^{high} particles can likely be detected at low particle concentrations, where the standard-loaded particles can no longer be recognized by the readout system, subsequent calculations have to be done with caution. Indeed, when comparing the penetration behavior of PAN and PAN-NR^{high}, both of similar size and composition but different Nile Red payload, PAN-NR^{high} but not PAN nanoparticles were detectable in the dermis. This is, as discussed above, likely not a dye-mediated enhancement of penetration, but a consequence of detection sensitivity. When comparing PAN-NR^{high} and P(ANcoNVP)24-NR^{high}, a trend towards enhanced penetration for more hydrophilic and flexible carriers may be concluded. In fact, flexible core-multishell

nanotransporters even surmount the stratum corneum barrier of human skin, if left in contact for 24 h [8].

Overall, a dependence of the individual size and hydrophilicity, defined by the specific matrix composition, on the skin penetration behavior of P(ANcoNVP) nanoparticles is indicated.

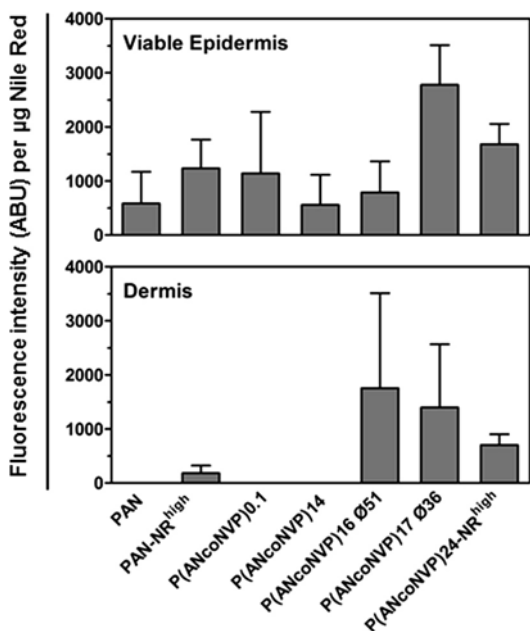


Figure 6. Penetration of Nile Red loaded P(ANcoNVP) nanoparticles in tape-stripped human skin. 90% stratum corneum of healthy human skin was removed by tape stripping and P(ANcoNVP) nanoparticles were applied for 6 h. Penetration behavior was evaluated using static-type Franz cells. Semi-quantitative data evaluation of arbitrary pixel brightness units (ABU) in the viable epidermis and dermis were used to estimate the amount of Nile Red. The final penetration value depicted as fluorescence intensity/ μg Nile Red was calculated according to the average intensity value, divided by the calculated amount of dye applied to the sample. Mean \pm SEM ($n = 3$).

Conclusion

Systematic variation of size and matrix composition of P(ANcoNVP) model nanoparticles allows gaining insights into critical criteria for the biocompatibility and functionality of copolymer nanoparticles. Using one set of materials rather than different material classes, these data indicate that varying hydrophilicity largely defines the interaction with NHK and NHDF, leading to differences in cell uptake and thus probably in biocompatibility. Moreover, it was shown that particles of 50 nm and smaller may penetrate into the dermis and possibly cause systemic effects by their payload in case of barrier-disrupted human skin. Hence, this study provided substantial information for plausible approaches to facilitate the transport of therapeutic drugs into the skin - as well as potential hazards induced by nanoparticles not intended to make contact with human skin.

In concordance with percutaneous drug penetration [60], the use of polymer-based nanoparticles of small size and a defined hydrophilic content indicated the strongest penetration enhancement. When aiming at a local therapy in barrier-disrupted skin with a low penetration depth, polymer nanoparticles of intermediate hydrophilicity and sizes in the range of 100 nm might be interesting to analyze in follow-up studies. By increasing lipophilicity or hydrophilicity, an enhanced cell uptake may be feasible to deliver therapeutic drugs into the cell, but may also be associated with decreased tolerability.

Conflict of interest

The authors declare that this article content has no conflicts of interest.

Acknowledgments

Technical support by Daniela Radzik, Andrea Pfeiffer, and Yvonne Pieper are acknowledged. This work was partially supported by the German Research Foundation (Collaborative Research Center 1112, projects A03, B03 and Z01) and the Federal Ministry of Education and Research, Germany (grant No. 1315848B). N.Z. gratefully acknowledges a doctoral scholarship from the China Scholarship Council. A.B. gratefully acknowledges an HONORS Fellowship from the Freie Universität Berlin.

References

- [1] S. Heilmann, S. Küchler, C. Wischke, A. Lendlein, C. Stein, M. Schäfer-Korting, A thermosensitive morphine-containing hydrogel for the treatment of large-scale skin wounds, *Int. J. Pharm.* 444 (2013) 96-102.
- [2] S.M. Shah, M. Ashtikar, A.S. Jain, D.T. Makhija, Y. Nikam, R.P. Gude, F. Steiniger, A.A. Jagtap, M.S. Nagarsenker, A. Fahr, LeciPlex, invasomes, and liposomes: a skin penetration study, *Int. J. Pharm.* 490 (2015) 391-403.
- [3] Z. Zhang, P.C. Tsai, T. Ramezanli, B.B. Michniak-Kohn, Polymeric nanoparticles- based topical delivery systems for the treatment of dermatological diseases, *Wiley Interdiscip. Rev. Nanomed. Nanobiotechnol.* 5 (2013) 205-218.
- [4] M.J. Santander-Ortega, T. Stauner, B. Loretz, J.L. Ortega-Vinuesa, D. Bastos- Gonzalez, G. Wenz, U.F. Schaefer, C.M. Lehr, Nanoparticles made from novel starch derivatives for transdermal drug delivery, *J. Control. Release* 141 (2010) 85-92.

- [5] Y. Zhai, G. Zhai, *Advances in lipid-based colloid systems as drug carrier for topic delivery*, *J. Control. Release* 193 (2014) 90-99.
- [6] Y. Yang, S. Sunoqrot, C. Stowell, J. Ji, C.-W. Lee, J.W. Kim, S.A. Khan, S. Hong, *Effect of size, surface charge, and hydrophobicity of poly(amidoamine) dendrimers on their skin penetration*, *Biomacromolecules* 13 (2012) 2154-2162.
- [7] J. Lademann, H. Richter, A. Teichmann, N. Otberg, U. Blume-Peytavi, J. Luengo, B. Weiss, U.F. Schaefer, C.M. Lehr, R. Wepf, W. Sterry, *Nanoparticles - an efficient carrier for drug delivery into the hair follicles*, *Eur. J. Pharm. Biopharm.* 66 (2007) 159-164.
- [8] N. Alnasif, C. Zoschke, E. Fleige, R. Brodewolf, A. Boreham, E. Rühl, K.M. Eckl, H.F. Merk, H.C. Hennies, U. Alexiev, R. Haag, S. Kuchler, M. Schäfer-Korting, *Penetration of normal, damaged and diseased skin-an in vitro study on dendritic core-multishell nanotransporters*, *J. Control. Release* 185 (2014) 45-50.
- [9] R. Neuman, S. Magdassi, Y. Milner, *Penetration and biological effects of topically applied cyclosporin A nanoparticles in a human skin organ culture inflammatory model*, *Exp. Dermatol.* 21 (2012) 938-943.
- [10] N. Vincent, D.D. Ramya, H.B. Vedha, *Progress in psoriasis therapy via novel drug delivery systems*, *Dermatol. Reports* 6 (2014) 5451.
- [11] R. Ghadially, J.T. Reed, P.M. Elias, *Stratum corneum structure and function correlates with phenotype in psoriasis*, *J. Invest. Dermatol.* 107 (1996) 558-564.
- [12] L.W. Zhang, W.W. Yu, V.L. Colvin, N.A. Monteiro-Riviere, *Biological interactions of quantum dot nanoparticles in skin and in human epidermal keratinocytes*, *Toxicol. Appl. Pharmacol.* 228 (2008) 200-211.
- [13] F. Rancan, Q. Gao, C. Graf, S. Troppens, S. Hadam, S. Hackbarth, C. Kembuan, U. Blume-Peytavi, E. Rühl, J. Lademann, A. Vogt, *Skin penetration and cellular uptake of amorphous silica nanoparticles with variable size, surface functionalization, and colloidal stability*, *ACS Nano* 6 (2012) 6829-6842.
- [14] F. Larese Filon, M. Mauro, G. Adami, M. Bovenzi, M. Crosera, *Nanoparticles skin absorption: new aspects for a safety profile evaluation*, *Regul. Toxicol. Pharmacol.* 72 (2015) 310-322.
- [15] S. Kumar, N. Alnasif, E. Fleige, I. Kurniasih, V. Kral, A. Haase, A. Luch, G. Weindl, R. Haag, M. Schäfer-Korting, S. Hedtrich, *Impact of structural differences in hyperbranched polyglycerol-polyethylene glycol nanoparticles on dermal drug delivery and*

- biocompatibility, *Eur. J. Pharm. Biopharm.* 88 (2014) 625-634.
- [16] C.F. Hung, W.Y. Chen, C.Y. Hsu, I.A. Aljuffali, H.C. Shih, J.Y. Fang, Cutaneous penetration of soft nanoparticles via photodamaged skin: lipid-based and polymer-based nanocarriers for drug delivery, *Eur. J. Pharm. Biopharm.* 94 (2015) 94-105.
- [17] R.V. Contri, L.A. Fiel, N. Alnasif, A.R. Pohlmann, S.S. Guterres, M. Schäfer- Korting, Skin penetration and dermal tolerability of acrylic nanocapsules: influence of the surface charge and a chitosan gel used as vehicle, *Int. J. Pharm.* 507 (2016) 12-20.
- [18] M. Morgen, G.W. Lu, D. Du, R. Stehle, F. Lembke, J. Cervantes, S. Ciotti, R. Haskell, D. Smithey, K. Haley, C. Fan, Targeted delivery of a poorly water- soluble compound to hair follicles using polymeric nanoparticle suspensions, *Int. J. Pharm.* 416 (2011) 314-322.
- [19] T.L. de Brum, L.A. Fiel, R.V. Contri, S.S. Guterres, A.R. Pohlmann, Polymeric nanocapsules and lipid-core nanocapsules have diverse skin penetration, *J. Nanosci. Nanotechnol.* 15 (2015) 773-780.
- [20] F. Rancan, D. Papakostas, S. Hadam, S. Hackbarth, T. Delair, C. Primard, B. Verrier, W. Sterry, U. Blume-Peytavi, A. Vogt, Investigation of polylactic acid (PLA) nanoparticles as drug delivery systems for local dermatotherapy, *Pharm. Res.* 26 (2009) 2027-2036.
- [21] S. Staufienbiel, M. Merino, W. Li, M.D. Huang, S. Baudis, A. Lendlein, R.H. Müller, C. Wischke, Surface characterization and protein interaction of a series of model poly[acrylonitrile-*co*-(*N*-vinyl pyrrolidone)] nanocarriers for drug targeting, *Int. J. Pharm.* 485 (2015) 87-96.
- [22] C. Wischke, A. Krüger, T. Roch, B.F. Pierce, W. Li, F. Jung, A. Lendlein, Endothelial cell response to (co)polymer nanoparticles depending on the inflammatory environment and comonomer ratio, *Eur. J. Pharm. Biopharm.* 84 (2013) 288-296.
- [23] A. Glinski, S. Liebel, È. Pelletier, C.L. Voigt, M.A.F. Randi, S.X. Campos, C.A. Oliveira Ribeiro, F. Filipak Neto, Toxicological interactions of silver nanoparticles and organochlorine pesticides in mouse peritoneal macrophages, *Toxicol. Mech. Methods* (2016) 1-9.
- [24] A. Jaeger, D.G. Weiss, L. Jonas, R. Kriehuber, Oxidative stress-induced cytotoxic and genotoxic effects of nano-sized titanium dioxide particles in human HaCaT keratinocytes, *Toxicology* 296 (2012) 27-36.
- [25] A. Boreham, T.Y. Kim, V. Spahn, C. Stein, L. Mundhenk, A.D. Gruber, R. Haag, P. Welker, K. Licha, U. Alexiev, Exploiting fluorescence lifetime plasticity in FLIM: target molecule

- localization in cells and tissues, *ACS Med. Chem. Lett.* 2 (2011) 724-728.
- [26] C. Richter, C. Schneider, M.T. Quick, P. Volz, R. Mahrwald, J. Hughes, B. Dick, U. Alexiev, N.P. Ernsting, Dual-fluorescence pH probe for bio-labelling, *Phys. Chem. Chem. Phys.* 17 (2015) 30590-30597.
- [27] A. Boreham, J. Pikkemaat, P. Volz, R. Brodewolf, C. Kuehne, K. Licha, R. Haag, J. Dervede, U. Alexiev, Detecting and quantifying biomolecular interactions of a dendritic polyglycerol sulfate nanoparticle using fluorescence lifetime measurements, *Molecules* 21 (2015) E22.
- [28] M. Witting, A. Boreham, R. Brodewolf, K. Vavrova, U. Alexiev, W. Friess, S. Hedtrich, Interactions of hyaluronic acid with the skin and implications for the dermal delivery of biomacromolecules, *Mol. Pharm.* 12 (2015) 1391-1401.
- [29] A. Boreham, M. Pfaff, E. Fleige, R. Haag, U. Alexiev, Nanodynamics of dendritic core-multishell nanocarriers, *Langmuir* 30 (2014) 1686-1695.
- [30] T.Y. Kim, K. Winkler, U. Alexiev, Picosecond multidimensional fluorescence spectroscopy: a tool to measure real-time protein dynamics during function, *Photochem. Photobiol.* 83 (2007) 378-384.
- [31] U. Alexiev, I. Rimke, T. Pohlmann, Elucidation of the nature of the conformational changes of the EF-interhelical loop in bacteriorhodopsin and of the helix VIII on the cytoplasmic surface of bovine rhodopsin: a time-resolved fluorescence depolarization study, *J. Mol. Biol.* 328 (2003) 705-719.
- [32] OECD, Test No. 437: Bovine Corneal Opacity and Permeability Test Method for Identifying (i) Chemicals Inducing Serious Eye Damage and (ii) Chemicals Not Requiring Classification for Eye Irritation or Serious Eye Damage, OECD Publishing.
- [33] W. Pape, Red Blood Cell Test System Invitox Protocol No. 37 ERGATT/FAME Databank of In Vitro Techniques in Toxicology, 1992.
- [34] M. Schäfer-Korting, U. Bock, W. Diembeck, H.J. Düsing, A. Gamer, E. Haltner-Ukomadu, C. Hoffmann, M. Kaca, H. Kamp, S. Kersen, M. Kietzmann, H.C. Korting, H.U. Krächter, C.M. Lehr, M. Liebsch, A. Mehling, C. Müller-Goymann, F. Netzlaff, F. Niedorf, M.K. Rübhelke, U. Schäfer, E. Schmidt, S. Schreiber, H. Spielmann, A. Vuia, M. Weimer, The use of reconstructed human epidermis for skin absorption testing: results of the validation study, *Altern. Lab. Anim.* 36 (2008) 161-187.
- [35] S. Lombardi Borgia, M. Regehly, R. Sivaramakrishnan, W. Mehnert, H.C. Korting, K.

- Danker, B. Röder, K.D. Kramer, M. Schäfer-Korting, Lipid nanoparticles for skin penetration enhancement-correlation to drug localization within the particle matrix as determined by fluorescence and piezoelectric spectroscopy, *J. Control. Release* 110 (2005) 151-163.
- [36] K. Landfester, M. Antonietti, The polymerization of acrylonitrile in miniemulsions: “Crumpled latex particles” or polymer nanocrystals, *Macromol. Rapid Commun.* 21 (2000) 820-824.
- [37] Y. Zhao, K.W. Ng, Nanotoxicology in the skin: how deep is the issue?, *Nano LIFE* 04 (2014) 1440004
- [38] K.J. Ong, T.J. MacCormack, R.J. Clark, J.D. Ede, V.A. Ortega, L.C. Felix, M.K.M. Dang, G. Ma, H. Fenniri, J.G.C. Veinot, G.G. Goss, Widespread nanoparticle- assay interference: implications for nanotoxicity testing, *PLoS ONE* 9 (2014) e90650.
- [39] A.L. Holder, R. Goth-Goldstein, D. Lucas, C.P. Koshland, Particle-induced artifacts in the MTT and LDH viability assays, *Chem. Res. Toxicol.* 25 (2012) 1885-1892.
- [40] A. Kroll, M.H. Pillukat, D. Hahn, J. Schnekenburger, Interference of engineered nanoparticles with in vitro toxicity assays, *Arch. Toxicol.* 86 (2012) 1123-1136.
- [41] X.W. Liang, Z.P. Xu, J. Grice, A.V. Zvyagin, M.S. Roberts, X. Liu, Penetration of nanoparticles into human skin, *Curr. Pharm. Des.* 19 (2013) 6353-6366.
- [42] V. Ölschläger, A. Schrader, S. Hockertz, Comparison of primary human fibroblasts and keratinocytes with immortalized cell lines regarding their sensitivity to sodium dodecyl sulfate in a Neutral Red uptake cytotoxicity assay, *Arzneimittelforschung* 59 (2009) 146-152.
- [43] M. Samadi Moghaddam, M. Heiny, V.P. Shastri, Enhanced cellular uptake of nanoparticles by increasing the hydrophobicity of poly(lactic acid) through copolymerization with cell-membrane-lipid components, *Chem. Commun. (Camb.)* 51 (2015) 14605-14608.
- [44] D.G. Deavall, E.A. Martin, J.M. Horner, R. Roberts, Drug-induced oxidative stress and toxicity, *J. Toxicol.* 2012 (2012) 13.
- [45] A. Manke, L. Wang, Y. Rojanasakul, Mechanisms of nanoparticle-induced oxidative stress and toxicity, *BioMed. Res. Int.* 2013 (2013) 15.
- [46] A. Onodera, F. Nishiumi, K. Kakiguchi, A. Tanaka, N. Tanabe, A. Honma, K. Yayama, Y. Yoshioka, K. Nakahira, S. Yonemura, I. Yanagihara, Y. Tsutsumi, Y. Kawai, Short-term changes in intracellular ROS localisation after the silver nanoparticles exposure depending

on particle size, *Toxicol. Rep.* 2 (2015) 574-579.

- [47] L. Wang, R.R. Mercer, Y. Rojanasakul, A. Qiu, Y. Lu, J.F. Scabilloni, N. Wu, V. Castranova, Direct fibrogenic effects of dispersed single-walled carbon nanotubes on human lung fibroblasts, *J. Toxicol. Environ. Health A* 73 (2010) 410-422.
- [48] A.R. Gliga, S. Skoglund, I.O. Wallinder, B. Fadeel, H.L. Karlsson, Size-dependent cytotoxicity of silver nanoparticles in human lung cells: the role of cellular uptake, agglomeration and Ag release, *Part. Fibre Toxicol.* 11 (2014) 11.
- [49] M.P. Vinardell, M. Mitjans, Alternative methods for eye and skin irritation tests: an overview, *J. Pharm. Sci.* 97 (2008) 46-59.
- [50] C. Eskes, S. Bessou, L. Bruner, R. Curren, J. Harbell, P. Jones, R. Kreiling, M. Liebsch, P. McNamee, W. Pape, M.K. Prinsen, T. Seidle, P. Vanparys, A. Worth, V. Zuang, Eye irritation, *Altern. Lab. Anim.* 33 (Suppl 1) (2005) 47-81.
- [51] OECD, Test No. 405: Acute Eye Irritation/Corrosion, OECD Publishing.
- [52] D.B. Warheit, R.A. Hoke, C. Finlay, E.M. Donner, K.L. Reed, C.M. Sayes, Development of a base set of toxicity tests using ultrafine TiO₂ particles as a component of nanoparticle risk management, *Toxicol. Lett.* 171 (2007) 99-110.
- [53] S. Hönzke, C. Gerecke, A. Elpelt, N. Zhang, M. Unbehauen, V. Kral, E. Fleige, F. Paulus, R. Haag, M. Schäfer-Korting, B. Kleuser, S. Hedtrich, Tailored dendritic core-multishell nanocarriers for efficient dermal drug delivery: a systematic top-down approach from synthesis to preclinical testing, *J. Control. Release* (2016), <http://dx.doi.org/10.1016/j.jconrel.2016.06.030> (Epub ahead of print).
- [54] C. Lotz, F.F. Schmid, A. Rossi, S. Kurdyn, D. Kampik, B. De Wever, H. Walles, F.K. Groeber, Alternative methods for the replacement of eye irritation testing, *Altex* 33 (2016) 55-67.
- [55] R.J. Scheuplein, I.H. Blank, Permeability of the skin, *Physiol. Rev.* 51 (1971) 702-747.
- [56] C.S.J. Campbell, L.R. Contreras-Rojas, M.B. Delgado-Charro, R.H. Guy, Objective assessment of nanoparticle disposition in mammalian skin after topical exposure, *J. Control. Release* 162 (2012) 201-207.
- [57] T.W. Prow, N.A. Monteiro-Riviere, A.O. Inman, J.E. Grice, X. Chen, X. Zhao, W.H. Sanchez, A. Gierden, M.A.F. Kendall, A.V. Zvyagin, D. Erdmann, J.E. Riviere, M.S. Roberts, Quantum dot penetration into viable human skin, *Nanotoxicology* 6 (2012) 173-185.

- [58] E. Proksch, J. Brasch, Abnormal epidermal barrier in the pathogenesis of contact dermatitis, *Clin. Dermatol.* 30 (2012) 335-344.
- [59] G. Cevc, D. Gebauer, J. Stieber, A. Schätzlein, G. Blume, Ultraflexible vesicles, transfersomes, have an extremely low pore penetration resistance and transport therapeutic amounts of insulin across the intact mammalian skin, *Biochim. Biophys. Acta* 1368 (1998) 201-215.
- [60] T. Higuchi, Physical chemical analysis of percutaneous absorption process from creams and ointments, *J. Soc. Cosmet. Chem.* 11 (1960) 85-97.